Electronic band structure of the two-dimensional metallic electron system Au/Ge(111)

P. Höpfner,[1] J. Schäfer,[1] A. Fleszar,[2] S. Meyer,[1] C. Blumenstein,[1] T. Schramm,[1] M. Heßmann,[1] X. Cui,[3] L. Patthey,[3] W. Hanke,[2] and R. Claessen[1]

[1]*Physikalisches Institut, Universität Würzburg, 97074 Würzburg, Germany*

[2]*Institut für Theoretische Physik und Astrophysik, Universität Würzburg, 97074 Würzburg, Germany*

[3]*Swiss Light Source, Paul-Scherrer-Institut, 5232 Villigen, Switzerland*

(Received 29 November 2010; revised manuscript received 13 April 2011; published 30 June 2011)

The two-dimensional electron system Au/Ge(111)-($\sqrt{3} \times \sqrt{3}$)$R30^\circ$ is studied in detail by angle-resolved photoemission and density functional theory calculations. In combining these results, we identify four metallic bands which are either of dominantly Au or Ge character, respectively. The largest Fermi surface sheet, originating from Au orbitals, is suggestive of a nesting condition due to its hexagonal shape. However, a charge density wave transition is not observed between room temperature and 10 K. The electronic structure obtained by density functional theory with inclusion of a self-energy correction is in good agreement with the experiment. These calculations also indicate that there is significant spin-orbit splitting, especially in the Au-related bands, which is partly of Rashba character.

DOI: 10.1103/PhysRevB.83.235435 PACS number(s): 73.20.At, 68.47.Fg, 71.15.Mb, 79.60.−i

I. INTRODUCTION

Confining electrons on surfaces represents an intriguing approach for the realization of two-dimensional (2D) electron systems. A common experimental procedure to create such a strictly defined situation is to deposit metallic adatoms in the submonolayer to monolayer (ML) thickness range onto a semiconducting substrate. This concept of generating a 2D electron system, depending on the choice of adatom-substrate combination in many cases succeeds in achieving adatom-induced surface states which are located in the band gap of the bulk density of states, so that a truly 2D confinement can be achieved.

The electronic properties of such systems can exhibit intriguing and oftentimes unexpected surprises. As a key example, for certain adatoms at low coverage, the electron localization will become significant, such that the electronic correlations are strongly increased. This phenomenon has recently developed into a topic of high impact ever since the observation of a temperature-induced Mott transition from the metallic to the insulating state in the ($\sqrt{3} \times \sqrt{3}$)-reconstructed surface of Sn/Ge(111).[1] Likewise, the related Sn/Si(111)-($\sqrt{3} \times \sqrt{3}$) surface was found to show similar characteristics with the opening of a surface band gap upon cooling.[2] Both results were further supported by theoretical calculations resting upon density functional theory (DFT) within the local density approximation, including local Coulomb interactions (LDA + U).[3]

Besides electron-electron correlation effects on these surfaces, there has been speculation about the formation of charge density waves (CDWs). The probability to observe such a transition is closely related to the topology of the room temperature Fermi surface. Basic requirements are parallel segments on the Fermi surface being connected by a nesting vector. An early and alleged example was believed to be the related Pb/Ge(111)-($\sqrt{3} \times \sqrt{3}$) surface, which initially was assumed to exhibit a CDW (3×3) ground state, additionally stabilized by electron-electron correlations.[4]

Detailed structural studies of Pb/Ge(111) have identified the transition into the low-temperature (3×3)-phase as a Jahn–Teller-type instability rather than a CDW transition.[5] Until today, a Peierls instability has not been unambiguously established in ($\sqrt{3} \times \sqrt{3}$)-reconstructed metal-semiconductor surfaces. This still spurs the thrust to search for CDWs in related surface systems with suitable Fermi surface topologies.

Many further open questions remain. For Sn/Ge(111), recent studies by scanning tunneling microscopy (STM) and scanning tunneling spectroscopy of the low-temperature gapped state have led to a debate over the results,[6] so that further experiments are required to understand the factors that play a role for enhanced electron correlations. The general idea is that by altering the choice of semiconducting substrate and metallic atom species, it should be possible to tune the degree of correlations in the 2D layer. In this way, different surface reconstructions with different electronic interactions may be generated. By adjusting the substrate-to-adlayer composition, it is possible to tune between highly correlated 2D electron systems, as e.g. Sn/Si(111), and quasifree 2D electron gases, with In/Si(111)-($\sqrt{7} \times \sqrt{3}$) as a prominent example.[7]

A second effect, in addition to electron correlations, is the spin-orbit interaction at surfaces, which may be rather different from the conventional bulk case. Here the presence of an asymmetry in the potential gradient towards the surface induces a specific spin-dependent splitting of the surface states, which is referred to as Rashba splitting.[8] Examples comprise metal surfaces with high atomic number Z such as Au(111) and Bi(111) and their surface alloys, e.g. Bi/Ag(111).[9–11] More generally, the occurrence of the Rashba spin-orbit interaction in semiconductors and their interfaces might be relevant for the development of semiconductor-based spintronics. So far, this has, for example, been reported for Bi/Si(111), Bi/Ge(111), Tl/Si(111), and thin Pb films on Si(111).[12–15] However, here the Rashba spin-split surface bands are completely occupied, thus rendering the surface insulating. Hence, it would be interesting to see whether deposition of other high-Z metals might induce spin-split surface states which are of metallic nature. To date, the only known example we are aware of is the β-phase of Pb/Ge(111).[16] It is thus highly desirable to explore the band topology and potential spin-orbit splittings of other candidate systems.

A novel and promising approach is to focus on noble-metal-covered semiconductors with a number of high-Z representatives. Examples comprise the adsorption of Ag on Si(111)[17,18] and the particularly heavy adatoms Au and Pt on the same substrate.[18–20] Among various surface reconstructions forming 2D electron systems on Si(111) upon metal deposition, the $(\sqrt{3} \times \sqrt{3})$-phase is the most common one. A corresponding system on Ge(111) is reported for Au, although it has been studied rarely during the past decades.[18,21,22] These previous reports are primarily concerned with structure, leaving the electronic properties still to be revealed.

The issues above relate to the interplay between correlations, spin physics, and charge ordering. One might even envision a Mott insulator scenario coexisting with a CDW, as has, for instance, been seen in 1T-$TaSe_2$.[23] Also, Rashba spin-split surface states might still be defined in a highly correlated surface system. The key technique for the exploration of these effects is angle-resolved photoelectron spectroscopy (ARPES), which allows us to obtain the necessary information on the electronic structure in k-space.

Here we report on the Au/Ge(111)-$(\sqrt{3} \times \sqrt{3})$ system in a combined experimental and theoretical approach. By using ARPES, the electronic band structure has been mapped. DFT calculations, which include a self-interaction correction for the Au states, reproduce the observed band structure well. We find several metallic bands which steeply disperse through the Fermi level, as seen experimentally along high-symmetry directions. One of these bands of Au origin exhibits a pronounced hexagonal Fermi surface, suggestive of Fermi-surface nesting, yet in testing the hypothesis of a CDW, no such experimental indications are found upon cooling. Regarding the DFT results, spin-orbit splitting is important. The predominantly Au-derived surface states show a large spin-orbit splitting, partly of the Rashba type.

The paper is organized as follows. After a review of the experimental procedure in Sec. II, we show results on the surface structure in Sec. III. The extensive results in Sec. IV comprise both the ARPES data as well as those from DFT. Subsequently, we discuss the findings and implications for the electronic properties in Sec. V before concluding in Sec. VI.

II. EXPERIMENT

Sample preparation was performed in an ultra-high vacuum chamber with a base pressure of 1×10^{-10} mbar. N-doped Ge(111) substrates were sputtered and annealed during several cycles to achieve a well-defined substrate, typically using 1.0 keV Ar^+-ions for 20 min, followed by annealing at ~900 °C for 30 s. After repeating this procedure 3–5 times, a sharp $c(8 \times 2)$ pattern was observed by low energy electron diffraction (LEED). One ML of Au was deposited by means of an electron beam evaporator with the sample held at room temperature. After a subsequent anneal at T ~700 °C, a high-quality $(\sqrt{3} \times \sqrt{3})$ pattern was obtained in LEED. The ARPES data were recorded in high-resolution studies down to 10 K at the Swiss Light Source, using the Surface and Interface Spectroscopy beamline (SIS) with the High-Resolution Photoemission Spectroscopy endstation (HRPES), which is equipped with a Scienta R 4000 analyzer. The setup provided a total resolution of 20 meV.

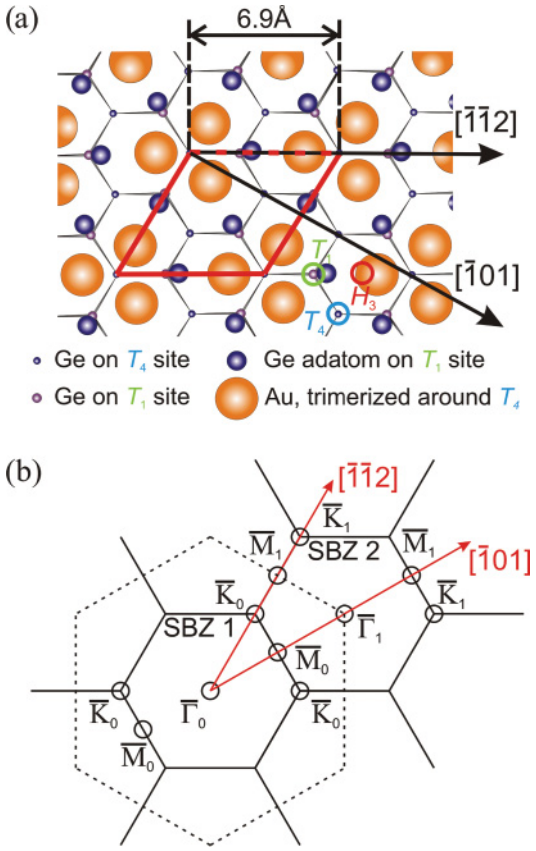

FIG. 1. (Color online) (a) Schematic drawing of the CHCT structural model for Au/Ge(111)-$(\sqrt{3} \times \sqrt{3})$. The dangling bonds of the topmost Ge bilayer are saturated by additional Ge adatoms. Au trimerizes around T_4 substrate sites. The $(\sqrt{3} \times \sqrt{3})$-unit cell is indicated by the parallelogram. (b) Sketch of reciprocal space geometries. $(\sqrt{3} \times \sqrt{3})$-SBZs boundaries are given by black lines, (1×1)-boundaries by dashed lines. $(\sqrt{3} \times \sqrt{3})$ symmetry points are marked by circles.

III. SURFACE STRUCTURE AND QUALITY

A. Structural model

The commonly accepted structural model of Au/Ge(111), as illustrated in Fig. 1(a), is the so-called conjugated honeycomb chained trimer (CHCT) model,[19] which has been confirmed by surface x-ray diffraction.[21] The dangling bonds of the Ge(111) substrate are saturated by additional Ge adatoms. As a prominent feature, Au atoms are arranged as trimers around T_4 sites with their apexes pointing towards H_3 sites. In this way, a $(\sqrt{3} \times \sqrt{3})$ surface reconstruction with 1 ML coverage is realized.

Starting from this commonly accepted structural model, one may attempt to derive an initial guess of the band filling. Such approach may be based on the method of electron counting, i.e. simply counting all unpaired electrons in the surface unit cell. In the present case, the three Au atoms per unit cell provide one 6s electron each, whereas Ge contributes nine electrons from sp^3 hybridized dangling bonds. In summing up these electrons, one obtains an even number of charge carriers. If taken at face value, this would suggest that each surface state is filled with two electrons, and consequently the surface should be insulating. However, this estimate is too simplistic because

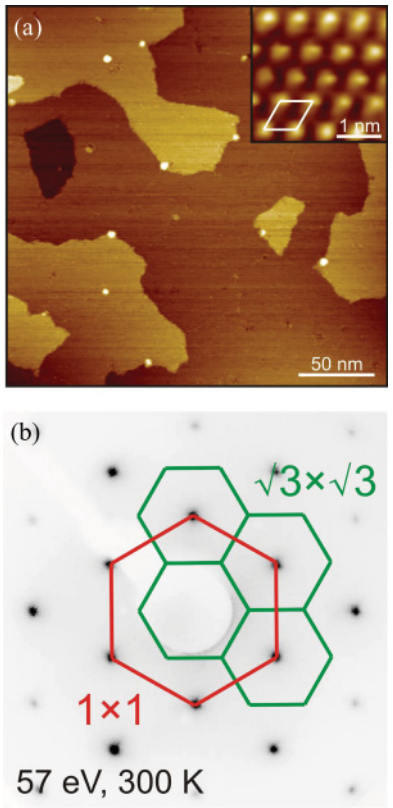

FIG. 2. (Color online) (a) Room temperature STM image of unoccupied states (+1.6 V, 0.5 nA) showing large area terraces of $(\sqrt{3} \times \sqrt{3})$-reconstructed Au/Ge(111). The inset presents a close-up to the atomic level (+1.2 V, 1.0 nA). The parallelogram indicates the unit cell. (b) LEED image with both (1×1) spots from the substrate and $(\sqrt{3} \times \sqrt{3})$ spots from the surface. SBZs are illustrated by hexagons.

it overlooks the possibility that multiple overlapping electron bands may exist which are only fractionally occupied, so that counting with integer electron numbers is not appropriate. Both the ARPES and DFT results below in Sec. IV(A) and (B), respectively, show that in fact the Au/Ge(111) system is indeed a metallic multiband system.

With regard to ARPES, which is a reciprocal space technique, the relevant symmetries shall be briefly addressed. The surface Brillouin zone (SBZ) is depicted in Fig. 1(b) for the $(\sqrt{3} \times \sqrt{3})$-reconstruction. For comparison, the (1×1) SBZ of the plain substrate is also indicated. The $[\bar{1}01]$ direction is defined by a line extending from the $\overline{\Gamma}_0$ point of the first SBZ to the $\overline{M}_0$ point at the zone boundary and includes the $\overline{\Gamma}_1$ point in the second SBZ. The $[\bar{1}\bar{1}2]$ direction extends from $\overline{\Gamma}_0$ to $\overline{K}_0$ at the corner between the first and second SBZs.

B. Quality of surface preparation

The existence of bands with well-defined dispersion $E(k)$ requires a long-range ordered surface with low defect density. The experimental ARPES data will be broadened if there is a huge amount of defects, step edges, or clusters of adsorbate or substrate atoms perturbing the structural order. As proof of the high quality of the surface preparation, Fig. 2(a) shows an STM image with large terraces (width >100 nm) of $(\sqrt{3} \times \sqrt{3})$-reconstructed Au/Ge(111), covering an area of 250×250 nm^2. Occasional small spots of bright intensity are assigned to Au clusters (diameter <5 nm) on the surface, yet the cluster density is still negligible. Point defects do not cover more than 2% of the surface area and thus should not influence the photoemission spectra significantly. The inset presents a close-up STM image at the atomic level, showing the $(\sqrt{3} \times \sqrt{3})$-surface reconstruction unit cell.

Furthermore, the LEED image in Fig. 2(b) reflects the regular array of $(\sqrt{3} \times \sqrt{3})$ spots together with the intense (1×1) spots of the underlying Ge(111) substrate. Judging from the marginal spot broadening and the low background level, we conclude that the surface is of high quality, and a sufficient degree of long-range order has been achieved.

IV. ELECTRONIC BAND STRUCTURE

A. Angle-resolved photoemission

In mapping the Fermi surface with ARPES at $T = 10$ K and at a photon energy $h\nu = 25$ eV, a metallic band H1 is observed in the central SBZ surrounding $\overline{\Gamma}_0$ in approximately starlike shape [see Fig. 3(a)]. The corners of the star are oriented towards the $\overline{K}_0$ points of the $(\sqrt{3} \times \sqrt{3})$ SBZ. Likewise, near $\overline{\Gamma}_0$ another surface state H2 with smaller contour is observed. This feature is rather weak in the first SBZ and very likely suppressed due to photoemission cross-section effects. Yet another state B1 is visible very close to $\overline{\Gamma}_0$. This band is assigned to the Ge bulk, as its energy position varies with photon energy, which reflects its k_z-dependence as typical of bulk states. Finally, the outermost Fermi surface sheet S1, seen here with moderate intensity, becomes very intense in the second SBZ, as in Fig. 3(b). Its contour is the largest in diameter, yet it exhibits a reduced extent in the $\overline{\Gamma}_1 - \overline{M}_1$ direction. It is interesting to note that the Fermi surface of S1 shows overall a roughly hexagonal shape.

For closer inspection of the band structure, it is mandatory to record the band dispersions $E(k_\parallel)$ along both high-symmetry directions. We begin with a high-resolution band map along $\overline{\Gamma}_0 - \overline{K}_0$ in Fig. 4(a) taken in the first SBZ, while we subsequently turn to the second SBZ in Fig. 4(b). A total of seven bands are observed. According to our DFT calculations, these can be classified as bulklike states (B), holelike surface states and resonances (H), and electronlike surface states and resonances (S). While interpreting the band map, Fig. 4(a) representing the first SBZ, one has to keep in mind that bulk-related features play a pronounced role here. Near $\overline{\Gamma}_0$ the steep parabolic band B1 crosses E_F, partially superimposing H3. Notably, the two bands H1 and H2 disperse up to E_F in parallel, spaced by an almost fixed k interval relative to each other. Turning to the surface states S1 and S2, they appear with comparatively faint intensity, as for example, the fully occupied state S2 with a band maximum at −350 meV binding energy and $k_\parallel = 0.43$ Å^{-1}.

The band structure along this $[\bar{1}\bar{1}2]$ high symmetry direction can also be accessed in the second SBZ (corresponds to $\overline{\Gamma}_1 - \overline{K}_1$), where the S1 band becomes more intense [see Fig. 4(b)]. In contrast to the holelike behavior of bands H1, H2, and H3, band S1 shows an electronlike behavior with approximately parabolic curvature. It has a band minimum at $\overline{\Gamma}_1$ and an occupied band width of ∼1 eV. However, it is significantly broadened. We determine a broadening

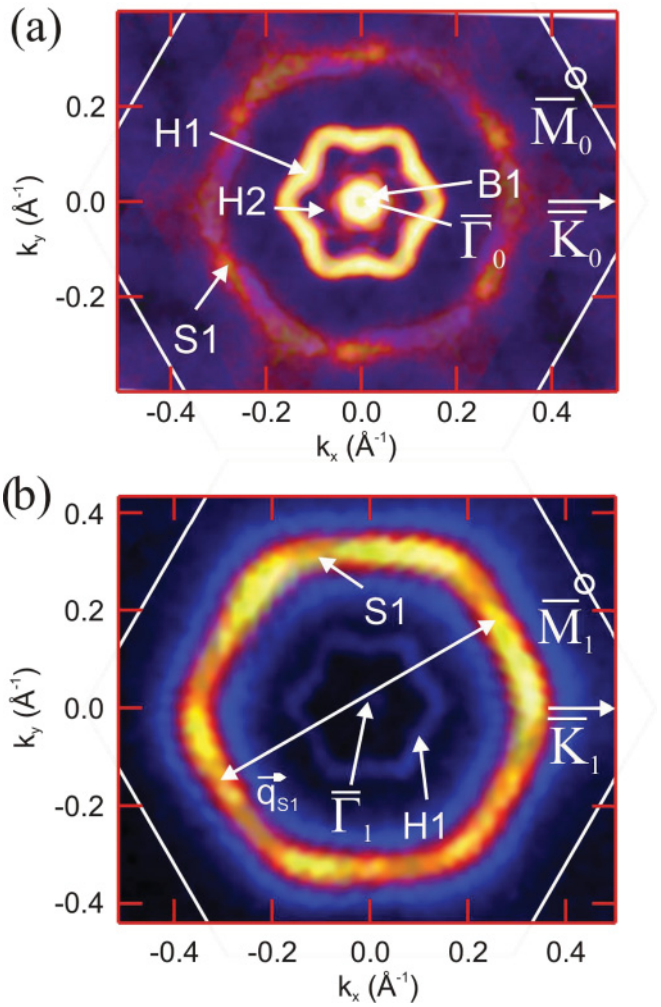

FIG. 3. (Color online) (a) Symmetrized ARPES Fermi surface in the first ($\sqrt{3} \times \sqrt{3}$) SBZ. Four Fermi surface sheets (S1, H1, H2, and B1) are indicated (S1 appearing suppressed); $T = 10$ K, $h\nu = 25$ eV. (b) Symmetrized Fermi surface in the second ($\sqrt{3} \times \sqrt{3}$) SBZ. S1 is strongly enhanced in contrast to the inner state H1, and H2 is completely suppressed; $T = 10$ K, $h\nu = 35$ eV.

of $\delta k_{\|} = 0.064$ Å^{-1} (full width at half maximum) of the momentum distribution curve at E_F, which clearly exceeds the experimental broadening. Yet, on a defect-free infinite surface, the spectral function $A(k, E)$ in ARPES should not show any intrinsic broadening at E_F. Thus, such width of the momentum distribution curve might relate to impurity scattering at surface defects. These can stem from occasional defects (e.g. Au-Ge exchange) or domain walls in the Au layer (registry shifts with respect to the substrate) that serve as scattering potential. Alternatively, the spectral function might be affected by electron correlations or result from an unresolved spin-orbit splitting. Our DFT results discussed below strongly suggest the spin-orbit splitting as the origin of the observed broadening of S1.

In contrast, the bands H1, H2, and H3 show up as weak and yet rather sharp streaks in the band map of the second SBZ [Fig. 4(b)]. This difference in intensities between first- and higher-order SBZs must again be ascribed to photoemission matrix element effects. Combining the data from both SBZs, Fermi-level crossings can be specified as 0.33 Å^{-1} for S1, 0.143 Å^{-1} for H1, and 0.072 Å^{-1} for H2 in the $\overline{\Gamma}_0 - \overline{K}_0$ direction.

For a complete view of the band structure, the $\overline{\Gamma}_0 - \overline{M}_0$ direction along [$\bar{1}$01] is shown in Fig. 5(a). In the first SBZ, one observes the same states as for the $\overline{\Gamma}_0 - \overline{K}_0$ direction. Likewise, H1, H2, and H3 appear more intense than the weak feature of S1. Following the curvatures of H1 and H2 from higher binding energies towards E_F, one observes a change from convex to concave band bending at $E_B \approx -150$ meV. As reported above, S1 exhibits an intense signal with broadened band dispersion in higher SBZs, as seen in the second SBZ in Fig. 5(b). For the $\overline{\Gamma}_0 - \overline{M}_0$ direction, one derives Fermi-level crossings at 0.31 Å^{-1} for S1, 0.117 Å^{-1} for H1, and 0.072 Å^{-1} for H2. In comparison with the k_F values for the $\overline{\Gamma}_0 - \overline{K}_0$ direction, S1 and H1 obey a hexagonal and modified hexagonal contour, respectively, as found in the Fermi surface mapping in Fig. 3.

With regard to this band situation with multiple Fermi-level crossings, this does not comply with the simple picture obtained by electron counting in Sec. III(A) that would predict an insulating behavior. From the Fermi surface data in Fig. 3,

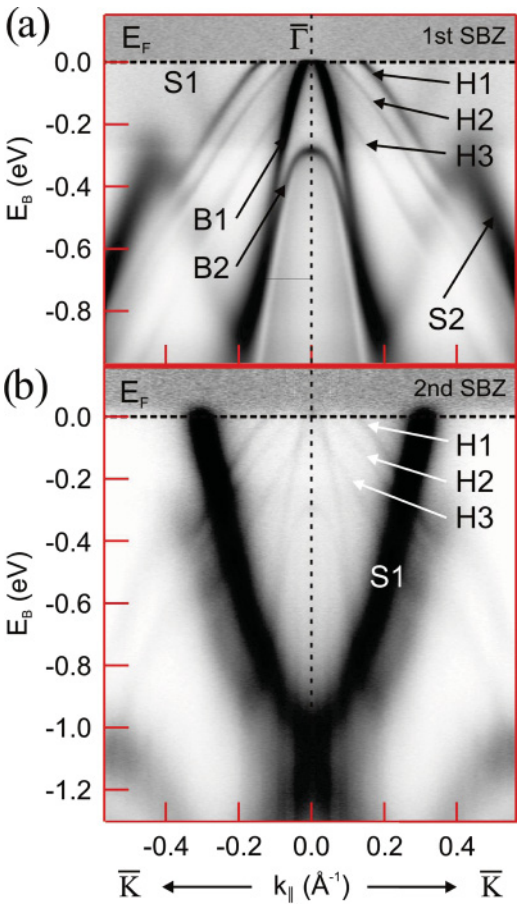

FIG. 4. (Color online) (a) Symmetrized band map along $\overline{\Gamma}_0 - \overline{K}_0$ direction in the first SBZ with states S1, S2, H1, H2, H3, and bulk states B1 and B2; $T = 10$ K, $h\nu = 25$ eV. (b) Symmetrized band map along the equivalent direction in the second SBZ. The S1 feature is strongly enhanced in contrast to the other bands; $T = 130$ K, $h\nu = 35$ eV (both band maps normalized to average energy distribution curve).

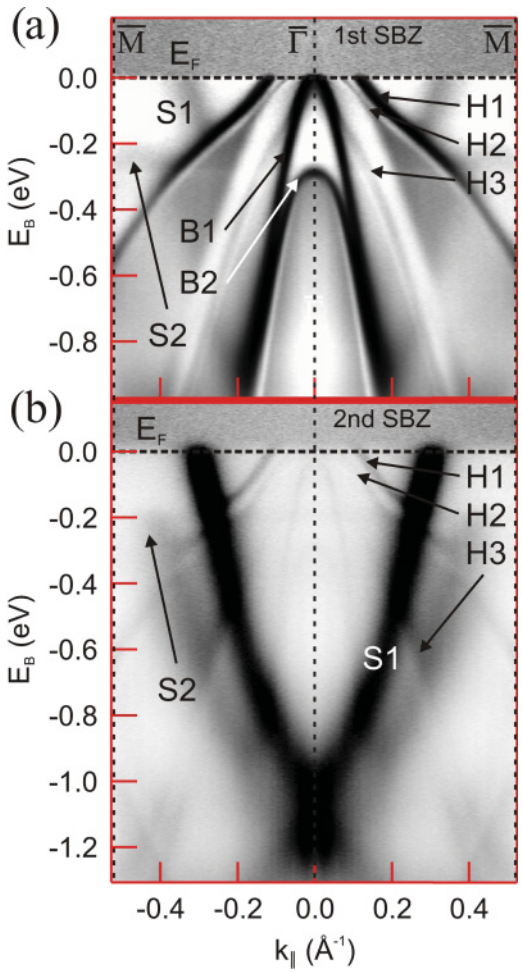

FIG. 5. (Color online) (a) Symmetrized band map along $\overline{\Gamma}_0 - \overline{M}_0$ direction in the first SBZ with states S1, S2, H1, H2, H3, and bulk states B1 and B2; $T = 10$ K, $h\nu = 25$ eV. (b) Symmetrized band map along the equivalent direction in the second SBZ. The S1 feature is strongly enhanced in contrast to the other bands; $T = 130$ K, $h\nu = 35$ eV (both band maps normalized to average energy distribution curve).

one can, for instance, derive a band filling of $\sim 1/3$ for S1, determined as a ratio between the occupied area fraction and the total SBZ area. The ARPES data likewise reveal a fractional occupation for the other surface bands, clearly indicating the limitations of such simple electron counting. Moreover, one finds electronlike and holelike bands, which relate to different orbital contributions to be discussed below in Sec. IV(B). We note in passing that the effective band mass of the electrons determined at the Fermi level as $m* = \hbar k_F / v_F$ with Fermi velocity v_F ranges from 0.05 to 0.09 m_e (in terms of the free electron mass m_e). These low values would suggest that Au/Ge(111) is a rather weakly correlated system, as opposed to strongly correlated systems with usually high band masses, e.g. Sn/Si(111). A plausible reason can be found in the threefold higher adatom density and the orbital character of the relevant surface states. In the highly correlated Sn/Si(111), the surface state stems from p_z-like dangling bonds, which are rather localized and have minimal overlap. Different from that, in Au/Ge(111) 6s orbitals play the dominant role. These have a much larger spatial extent and in conjunction with the higher atomic packing density thus lead to a greater overlap. Therefore, electron-electron correlations ought to be of minor importance here.

B. Density functional theory

Based upon the CHCT structural model, we also performed density functional calculations within the local density approximation (LDA).[24] The algorithm utilized a periodic slab system composed of one layer of Au atoms on the surface followed by 19 Ge layers and terminated by a hydrogen layer on the backside. The extent of the vacuum gap is 7.7 Å, which ensures that there is no overlap of wave functions from neighboring slabs. The calculations have been carried out within a mixed-basis code in which in addition to plane waves also localized Gaussian functions of angular momentum $l = 2$ have been placed at the positions of the Au atoms.[25]

It turns out that the electronic structure obtained within the standard LDA approach, although already reproducing the experimental results reasonably, still significantly underestimates the binding energy (and hence the band minimum) of the predominantly Au-derived quasiparabolic S1 band. In order to test a structure-related origin, calculations were done for many other structural models, yet they resulted in both less compatible electronic structures with regard to the experiment, as well as in higher surface formation energies. Instead, discrepancies will thus relate to the inherent shortcomings of the DFT method. Amongst these, the self-interaction error plays the most pronounced role, affecting particularly the quite localized 5d states of Au. They participate in the bonding with the Ge surface and are energetically situated very close to E_F. In order to include the self-interaction correction (SIC), similarly as in our previous work on II-VI compounds,[26,27] we have modified the d part of the Au LDA pseudopotential such that the band structure obtained for bulk Au agrees well with corresponding photoemission measurements.

The calculated band structure for Au/Ge(111) in both high-symmetry directions is shown in Fig. 6. Most of the states observed in the ARPES experiment are well reproduced. The Fermi level has been shifted upwards by +110 meV to achieve better agreement with the Fermi vectors of the H1 band. We attribute this to an excess charge concentration at the surface due to doping by surplus Au adatoms, which slightly increases the total charge per unit cell. Concerning the exact positions of k_F values, there are only minor deviations from the experimental results. These are $\Delta k_\parallel = -0.045$ Å^{-1} for S1 and -0.004 Å^{-1} for H1 in the $\overline{\Gamma} - \overline{M}$ direction. Along $\overline{\Gamma} - \overline{K}$, the corresponding values are $\Delta k_\parallel = -0.045$ Å^{-1} for S1 and $+0.004$ Å^{-1} for H1. This implies a rather good agreement with the experiment.

Furthermore, DFT provides essential information about the origin of the observed bands. The assignment relies on the integrated charge of a given state in dependence on the depth below the surface and its k value. For instance, a charge concentration of more than 50% in the topmost layer (Au) for one band is associated with a state being mainly derived from Au orbitals. It turns out that H states are predominantly Ge derived, whereas S states (S1 and S2) are mostly Au derived. Moreover, the incorporation of the SIC helps to reproduce the mainly Au-derived surface state S1 more exactly than standard

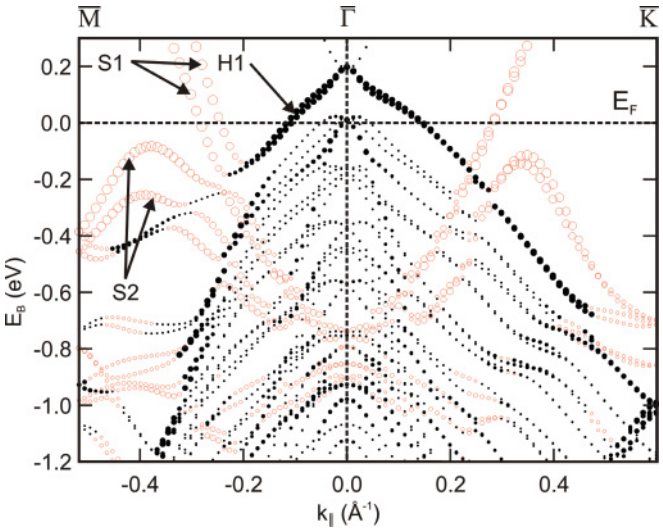

FIG. 6. (Color online) (a) Calculated band structure along $\overline{\mathrm{M}} - \overline{\Gamma} - \overline{\mathrm{K}}$. Red and black circles represent predominantly Au- and Ge-derived states, respectively. Their size indicates the surface (large) versus bulk (small) character as deduced from the resulting wave functions. Both S1 and S2 are spin-orbit-split bands, whereas H1 shows a smaller splitting. The Fermi level is shifted by +110 meV to achieve better agreement with experiment.

LDA. However, there still remains a difference in the occupied bandwidth of slightly more than 0.2 eV with regard to the experiment.

DFT also provides an interesting result concerning the spin character of the bands. The S1 band is predicted to be spin-orbit split by $\Delta k_R = 0.040$ Å^{-1} with a partial contribution to the splitting coming from the Rashba-type asymmetry of the potential gradients. This is an important hint towards an explanation of the strong broadening in the experiment, Fig. 5(b), as an unresolved splitting. Moreover, S2 is likewise spin split. This band also appears as a rather broad feature in the ARPES data. According to the calculations, the H1 band shows a spin-orbit splitting, too. It is rather small but has almost entirely the Rashba-type character.

V. DISCUSSION

The results presented in the preceding sections contain a series of interesting aspects which are addressed in the following. The ARPES data represent a novel example of a noble-metal-induced 2D electron system on a semiconductor substrate that shows metallic character. Moreover, the Fermi surface topology has a remarkable shape. The roughly hexagonal contour of S1 in Fig. 3(b) indicates potential Fermi-surface nesting. The occurrence of parallel sections in the Fermi surface, which may be connected by a nesting vector, is a mandatory precondition for the formation of a CDW at low temperature. Such a transition comprises a lattice distortion combined with a charge redistribution, which results in a band backfolding and the opening of a small band gap at new SBZ boundaries.[28] The susceptibility of a system for CDW instability strongly depends on the interplay between energy cost for the lattice distortion and electronic energy gain by the opening of an energy gap. A favorable situation oftentimes exists in the case of commensurate nesting, i.e. when the distortion period in real space is an integer of the surface lattice constant a_0.

In the case of Au/Ge(111), there exist roughly parallel sections of the Fermi contours, which may be connected by a nesting vector $q_{S1} = 0.62$ Å^{-1} [see Fig. 3(b)]. (This consideration ignores the spin splitting seen in DFT). Due to the threefold rotational symmetry of the surface, three equivalent nesting vectors exist, each rotated by 120°. This corresponds to a superstructure period of 2.9 a_0 in real space. However, this noninteger value does not coincide with any multiple of the periodicity of the $(\sqrt{3} \times \sqrt{3})$-reconstructed surface nor with a larger unit cell superstructure. Therefore, the formation of a CDW is rather unlikely. Experimentally, based on photoemission performed between $T = 10$ K and $T = 300$ K (not shown), which did not reveal any sign of a band backfolding, we may exclude such a CDW transition for Au/Ge(111). Rather, a lack of lock-in energy between a potential CDW and the lattice, due to the incommensurate nesting vector, seems to hinder the formation of such superstructure. This mechanism has also been invoked for the absence of a CDW in the related dense β-phase of Pb/Ge(111).[29] Furthermore, the electronic susceptibility $\chi_0(\vec{q})$ is a measure of the response of the electron gas to an external perturbation. Singular behavior at a particular wave vector $\vec{q}$ signals a potential CDW instability. According to a theoretical treatment on the related surfaces Sn/Ge(111) and Pb/Ge(111), $\chi_0(\vec{q})$ does not peak at (3×3) zone boundaries and thus does not support a CDW formation.[30] Eventually, the rigidity of the surface lattice can influence the probability to observe a CDW, too. Here, among other factors, the cohesion energy of an atom species is an indicator of the energetic stability. In the case of Au, we deal with rather large values (5.8 eV) and thus strong interatomic bonds.[31] This may also favor the absence of CDW formation in Au/Ge(111).

Another important point of interest is the origin of the holelike H states. In ARPES they are barely observable in higher SBZs, due to low photoemission matrix elements. DFT reveals that these bands are predominantly Ge-derived states. The H1 state is located a few layers below the surface in the slab. For H2 and H3, seen in ARPES faintly, we find in DFT a significant delocalization of the wave functions in this k region into the bulk. This suggests that the states are surface resonances that overlap with the Ge bulk band projection which is represented by the slab calculation.

Our finding of effective band masses in the range between 0.05 m_e and 0.09 m_e makes Au/Ge(111) a promising candidate for high-mobility electron transport in two dimensions ($\mu \propto 1/m^*$). Almost identical values are reported for the related Ag/Si(111) with 0.07 m_e and with a slightly higher mass for Au/Si(111) with 0.25 m_e.[17] These findings of low effective masses might stimulate further research towards semiconductor-based electronic applications resting on these low-dimensional surface systems.

According to our DFT calculations, spin-orbit interaction plays a major role in Au/Ge(111). Compared to the states H1, H2, and H3, band S1 is strongly broadened. Although a band splitting of S1 as predicted by the DFT is not resolved in experiment, its theoretical value accounts for most of the experimental width of this state. The band broadening of S1 in ARPES is the same everywhere along the Fermi surface.

This is fully consistent with DFT when viewing this as a small unresolved spin-orbit splitting. The calculation finds a persistent spin-orbit splitting of constant magnitude for all 2D k-space directions, while only in very close vicinity to the $\overline{\Gamma} - \overline{\mathrm{K}}$ direction this splitting becomes smaller.

In comparing the present Au/Ge(111) system to other metal adsorbates on Ge(111) at 1 ML coverage, the Pb/Ge(111)-$(\sqrt{3} \times \sqrt{3})$ reconstruction comes to mind[32] (not to be confused with the dilute 1/3 ML α-phase[4]). In that ARPES study, bands at the $\overline{\Gamma}$ point with holelike dispersions, which bear close resemblance to the H states in Au/Ge(111), were also attributed to Ge-derived states.

Regarding other noble metal adlayers in $(\sqrt{3} \times \sqrt{3})$-reconstruction, Pt/Si(111) is described by a slightly modified CHCT model.[20] Unlike in Au/Ge(111), a symmetry-breaking arrangement of Pt trimers renders this system an example of a chiral surface. Further related systems are Au/Si(111) and Ag/Si(111), which have been studied by ARPES.[17] Both surfaces exhibit metallic quasiparabolic bands. However, in the Ag system metallicity is induced upon doping only, for example, by providing excess Au or Ag atoms. In Au/Si(111), formation of very small domains is noted,[33] which prohibits long-range order and which will affect the quality of any ARPES data. Nonetheless, an adatom-induced band has been observed which resembles our predominantly Au-derived band S1.[17] In addition, the authors of Ref. 17 find a small electron pocket at the $\overline{\Gamma}$ point, for which there is no correspondence in the current data and which may be doping induced.[17]

VI. CONCLUSIONS

In summary, we have shown that a monolayer of Au on the (111) surface of Ge induces a metallic $(\sqrt{3} \times \sqrt{3})$-reconstruction. Fermi-surface mapping reveals a hexagonal shape of the largest Fermi sheet, which is suggestive of nesting. However, in the temperature range from 300 K down to 10 K, no CDW transition is observed, which is probably due to a lack of lock-in energy since the nesting vector is incommensurate with the underlying substrate. Moreover, the observed states show rather sizeable dispersions with low effective electron masses. This latter finding might be a desirable ingredient for future high-mobility electron transport applications.

Density functional theory agrees well with the experiment and allows us to determine the orbital origin of the bands as mainly derived from surface Au atoms, surface Ge atoms, or the Ge bulk. In addition, valuable insight into the role of the spin-orbit interaction at the Au/Ge(111) surface is obtained. According to the calculated band structure, there is a large splitting in the predominantly Au-derived surface state, which calls for further investigation, e.g. by spin-resolved photoemission.

ACKNOWLEDGMENTS

This work was supported by the DFG (Grants Scha 1510/2-1, Ha 1537/22-1, and FOR 1162) and the EU Framework Program FP7/2007-2013 (Grant 226716). The calculations have been done at the supercomputers of the Forschungszentrum Jülich within the HWB03 project.

[1] R. Cortés, A. Tejeda, J. Lobo, C. Didiot, B. Kierren, D. Malterre, E. G. Michel, and A. Mascaraque, Phys. Rev. Lett. **96**, 126103 (2006).
[2] S. Modesti, L. Petaccia, G. Ceballos, I. Vobornik, G. Panaccione, G. Rossi, L. Ottaviano, R. Larciprete, S. Lizzit, and A. Goldoni, Phys. Rev. Lett. **98**, 126401 (2007).
[3] G. Profeta and E. Tosatti, Phys. Rev. Lett. **98**, 086401 (2007).
[4] J. M. Carpinelli, H. H. Weitering, E. W. Plummer, and R. Stumpf, Nature **381**, 398 (1996).
[5] A. Mascaraque, J. Avila, J. Alvarez, M. C. Asensio, S. Ferrer, and E. G. Michel, Phys. Rev. Lett. **82**, 2524 (1999).
[6] S. Colonna, F. Ronci, A. Cricenti, and G. Le Lay, Phys. Rev. Lett. **101**, 186102 (2008).
[7] E. Rotenberg, H. Koh, K. Rossnagel, H. W. Yeom, J. Schäfer, B. Krenzer, M. P. Rocha, and S. D. Kevan, Phys. Rev. Lett. **91**, 246404 (2003).
[8] Yu. A. Bychkov and E. I. Rashba, JETP Lett. **39**, 78 (1984).
[9] S. LaShell, B. A. McDougall, and E. Jensen, Phys. Rev. Lett. **77**, 3419 (1996).
[10] Y. M. Koroteev, G. Bihlmayer, J. E. Gayone, E. V. Chulkov, S. Blügel, P. M. Echenique, and Ph. Hofmann, Phys Rev. Lett. **93**, 046403 (2004).
[11] C. R. Ast, D. Pacilé, L. Moreschini, M. C. Falub, M. Papagno, K. Kern, M. Grioni, J. Henk, A. Ernst, S. Ostanin, and P. Bruno, Phys. Rev. B **77**, 081407 (2008).
[12] I. Gierz, T. Suzuki, E. Frantzeskakis, S. Pons, S. Ostanin, A. Ernst, J. Henk, M. Grioni, K. Kern, and C. R. Ast, Phys. Rev. Lett. **103**, 046803 (2009).
[13] S. Hatta, T. Aruga, Y. Ohtsubo, and H. Okuyama, Phys. Rev. B **80**, 113309 (2009).
[14] K. Sakamoto, T. Oda, A. Kimura, K. Miyamoto, M. Tsujikawa, A. Imai, N. Ueno, H. Namatame, M. Taniguchi, P. E. J. Eriksson, and R. I. G. Uhrberg, Phys. Rev. Lett. **102**, 096805 (2009).
[15] J. H. Dil, F. Meier, J. Lobo-Checa, L. Patthey, G. Bihlmayer, and J. Osterwalder, Phys. Rev. Lett. **101**, 266802 (2008).
[16] K. Yaji, Y. Ohtsubo, S. Hatta, H. Okuyama, K. Miyamoto, T. Okuda, A. Kimura, H. Namatame, M. Taniguchi, and T. Aruga, Nat. commun. **1**, 17 (2010).
[17] J. N. Crain, K. N. Altmann, C. Bromberger, and F. J. Himpsel, Phys. Rev. B **66**, 205302 (2002).
[18] J. Nogami, K. Wan, and J. C. Glueckstein, Jpn. J. Appl. Phys. **33**, 3679 (1994).
[19] Y. G. Ding, C. T. Chan, and K. M. Ho, Surf. Sci. **275**, L691 (1992).
[20] P. Höpfner, M. Wisniewski, F. Sandrock, J. Schäfer, and R. Claessen, Phys. Rev. B **82**, 075431 (2010).
[21] P. B. Howes, C. Norris, M. S. Finney, E. Vlieg, and R. G. van Silfhout, Phys. Rev. B **48**, 1632 (1993).
[22] L. Seehofer and R. L. Johnson, Surf. Sci. **318**, 21 (1994).
[23] P. Fazekas and E. Tosatti, Philos. Mag. B **39**, 229 (1979).
[24] P. Hohenberg and W. Kohn, Phys. Rev. B **136**, B864 (1964).
[25] A. Fleszar, M. Potthoff, and W. Hanke, Phys. Status Solidi C **4**, 3270 (2007); A. Fleszar, W. Hanke, W. Weigand, C. Kumpf, C. Heske, E. Umbach, L. Plucinski, and R. L. Johnson, *ibid.* **4**, 3204 (2007).
[26] A. Fleszar and W. Hanke, Phys. Rev. B **71**, 045207 (2005).

[27] A. Fleszar and W. Hanke, Phys. Rev. B **56**, 12285 (1997).
[28] J. Schäfer, D. Schrupp, E. Rotenberg, S. D. Kevan, and R. Claessen, Appl. Phys. A **80**, 965 (2005).
[29] H. Morikawa, I. Matsuda, and S. Hasegawa, Phys. Rev. B **77**, 193310 (2008).
[30] G. Santoro, S. Scandolo, and E. Tosatti, Phys. Rev. B **59**, 1891 (1999).
[31] F. Kajzar and J. Mizia, J. Phys. F: Met. Phys. **7**, 1115 (1977).
[32] S. J. Tang, T. R. Chang, C. C. Huang, C. Y. Lee, C. M. Cheng, K. D. Tsuei, H. T. Jeng, and C. Y. Mou, Phys. Rev. B **81**, 245406 (2010).
[33] T. Nagao, S. Hasegawa, K. Tsuchie, S. Ino, C. Voges, G. Klos, H. Pfnür, and M. Henzler, Phys. Rev. B **57**, 10100 (1998).